Boundary-induced patterns in excitable systems: The structure of oscillatory domain

Olga Nekhamkina and Moshe Sheintuch
Department of Chemical Engineering, Technion, Israel Institute of Technology, Haifa 32000, Israel
(Received 12 November 2006; revised manuscript received 12 February 2007; published 18 May 2007)

The present work extends our recently published study [Phys. Rev. E **73**, 066224 (2006)] on a mechanism of pattern formation in excitable media due to inhomogeneous boundary conditions (BC). To that end, we analyze a pair of coupled excitable and oscillatory cells, a distributed FitzHugh Nagumo model, and a distributed five-variable model that describes CO catalytic oxidation. For the three systems we determine the structure of the oscillatory domains, composed of bands of complex firing solutions with period-adding bifurcations, and show the commonality of the structures. The obtained results account for the recently reported experimental observations of mixed-mode oscillations showing a period-adding bifurcation during CO oxidation on a disk-shaped catalytic cloth with imposed cold temperature BC.

DOI: 10.1103/PhysRevE.75.056210 PACS number(s): 05.45.−a, 47.54.−r, 82.40.Bj

I. INTRODUCTION

In a recent study [1] we showed that inhomogeneous boundary conditions (BC) in a distributed reaction-diffusion excitable systems are a natural source of permanent perturbations, that can induce wave trains which can be characterized as mixed-mode spatiotemporal oscillations showing a period-adding bifurcation sequence when a parameter is varied. The present work extends this mechanism of complex spatiotemporal pattern formation and outlines the structure of the sustained solutions in the parameter plane.

Pattern formation in both discrete and distributed excitable systems were intensively studied in the past decade. A single stimulated excitable cell (EC) governed by slow and fast state variables, and subject to external periodic stimuli was shown to exhibit a sequence of period-adding bifurcations in the limiting case of large time scale separation; the temporal behavior becomes even more complex in the case of a finite time scale ratio [2]. Complex types of the EC patterns, including frequency-locking and chaotic behavior, were also studied in Refs. [3–5]. Ensembles of EC and self-oscillatory cells (OC) can exhibit several scenarios of global system excitation due to local sources [6–9]. In our previous study [1] we considered a minimalistic model composed of a pair of EC and OC, both governed by an *S*-shaped source function [FitzHugh-Nagumo (FHN) system] with somewhat different parameters. (Complex patterns can be obtained in a pair of identical excitable FHN elements only in the case of repulsive coupling [10] which implies negative diffusivity.) We have demonstrated that such a system may exhibit both a regular solution of $1:n$ form (i.e., one EC oscillation corresponds to n OC oscillations) as well as complex and even chaotic behavior.

While the coupled EC/OC is a simple and natural system, since one expects to find oscillatory behavior in an excitable system subject to inhomogeneous BC, the pattern in a distributed system is more complex as it depends on the ability of the system to convey the wave and its fate (reflection or absorption) when reaching the opposite edges. Most studies of pattern formation in the distributed excitable media were conducted for unbounded homogeneous media and were aimed mainly at derivation of the dispersion relation between the wave speed and the pulse wavelength [11–13]. In the case of inhomogeneous systems the efforts were focused on complex pattern formation due to either noise effects [14,15] or due to different types of localized oscillation sources and spatial inhomogeneities [16–18]. While various complex patterns were obtained in these studies including regular and aperiodic mixed-mode type oscillations, no regular bifurcation sequence was detected upon varying a system parameter. In a recent study [19], a resonance-induced pacemaker was proposed as a new source of successive traveling waves in excitable media. This mechanism was illustrated experimentally as well as numerically for the photosensitive Belousov-Zhabotinsky reaction stimulated periodically by light. The sustained patterns exhibit mixed-mode oscillations and admit a period-adding bifurcation with varying external light frequency.

Boundary conditions are a natural source of permanent perturbations in distributed excitable or oscillatory systems and can induce complex patterns without any external forcing [20–23]. While our recent study [1] of moving wave trains, which can be temporally characterized as mixed-mode oscillations undergoing a period-adding bifurcation sequence revealed patterns qualitatively similar to those in Ref. [19], the source is not due to imposed external forcing (as in [19]), but due to the imposed inhomogeneous BC. Aside from the coupled EC/OS system we simulated in [1] a distributed FitzHugh Nagumo model and a distributed five-variable model that describes thermal patterns during catalytic CO oxidation at atmospheric pressure as in the experimental results [25] that motivated this study.

In this work we approximate the continuous extended models to show the similarity with the EC/OC system. The main focus in the present work is on the analysis of the oscillatory domain (OD) structure in the parameter space and the detection of the threshold parameters that ensures the complex system behavior. The obtained results showing the similarity of the main features for all models allow us to conclude that the proposed mechanism of spatiotemporal pattern formation due to inhomogeneous BC is really a general mechanism which may be applied to any excitable system.

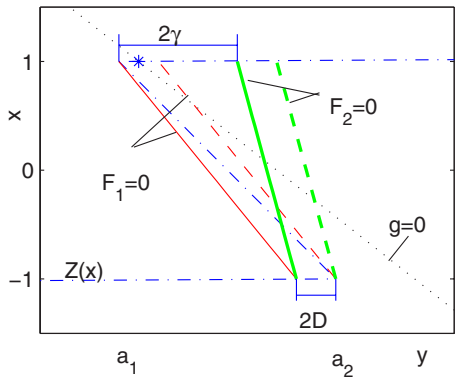

FIG. 1. (Color online) Coupled cells model [Eqs. (1)–(4)]. Phase plane shows source function $Z(x)$ (dash-dotted line), null cline $g(x,y)=0$ (dotted line), and the intermediate branches of null clines $F_i(x_i,y_i)=0 (i=1,2)$ of cell 1 (thin) and 2 (thick lines), respectively. Solid and dashed lines F_i for each cell are shown for the case that the other cell belongs to the upper (solid) and lower (dashed) branches, respectively. The star marks a fixed point of the isolated cell.

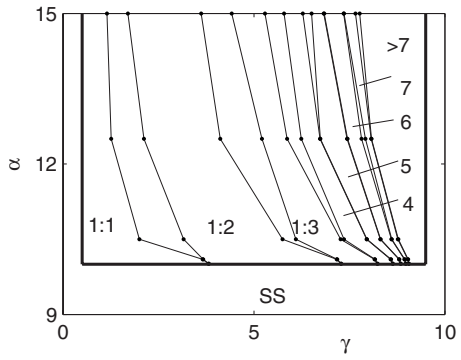

FIG. 2. Coupled cells model [Eqs. (1)–(4)]. Typical structure of the oscillatory solutions in the (γ,α) plane showing subdomains of regularly locked $1:n$ solutions separated by gaps of complex (chaotic) behavior. Solutions up to 1:7 are traced. $a_1=-1$, $a_2=20$, $\alpha=12.5$, $D=1$, $x_w=-1$. SS denotes the steady state solution.

The structure of this paper is as follows. In the next section the minimalistic discrete EC/OC system is described. In the following two sections the distributed FitzHugh Nagumo model and the distributed five-variable model that describes CO catalytic oxidation are considered. In the last section we discuss the similarity and the distinction of these models.

II. PAIR OF COUPLED AN EXCITABLE AND OSCILLATORY CELLS

Consider a pair of coupled excitable (1) and oscillatory (2) cells which are governed by a caricature of the FHN model with a piecewise-linear nonlinearity: This can be considered as a minimalistic discrete model which incorporates the boundary conditions by affecting the governing system:

$$\dot{x_1} = y_1 - Z(x_1) - D(x_1 - x_2) = F_1(x_i, y_1), \tag{1}$$

$$\dot{x_2} = y_2 - Z(x_2) + D(x_1 - x_2) - \gamma(x_2 - x_w) = F_2(x_i, y_2), \tag{2}$$

$$\dot{y_i} = \varepsilon[-\alpha(x_i - 1) - y_i] = g(x_i, y_i), \quad i = 1,2, \tag{3}$$

$$Z(x) = \begin{cases} a_2 + (x+1)/\delta, & x \in (-\infty, -1], \\ a_2 - 0.5(a_2 - a_1)(x+1), & x \in (-1, 1), \\ a_1 + (x-1)/\delta, & x \in [1, \infty), \end{cases} \tag{4}$$

with $\varepsilon, \delta \ll 1$ (see Ref. [1] for details). We assume that the fixed point of a single isolated cell (x_s, y_s, with $D=\gamma=0$) is excitable and x_w belongs to the branch opposite of x_s (Fig. 1). The additional term in Eq. (2) $[\gamma(x_2 - x_w)]$ mimics the effect of BC and ensures shifting of the phase plane of cell 2 towards the oscillatory state. In the limiting case of $\varepsilon \to 0$, $\delta \to 0$ system (1)–(4) can be simplified further and reduced to a binary model. In this case the system spends all of its time on the stable (upper or lower) branches $Z(x)$ with $x_i = +1$ or -1, respectively (Fig. 1). Now the phase planes of each cell can be constructed in a simple way when accounting for the state variable x of the other cell. The limit points of the null-curve of cell 1 (y_1^{LP}) coincide with those of $Z(x)$ if both cells move along the same branch and are shifted by 2D if the cells belong to opposite branches. The limit points of the phase plane of cell 2 (y_2^{LP}) get additional shifting at the upper branch by 2γ due to the external forcing. We assume that due to interaction cell 1 can be shifted to the oscillatory state, while the phase plane type of cell 2 is preserved. Simple geometrical considerations allow us to derive the following conditions for the governing parameters:

$$\begin{aligned} &y_s - a_1 < 2\gamma < a_2 - a_1 - 2\mathrm{D}, \\ &y_s - a_1 < 2\mathrm{D} < a_2 - a_1 - 2\gamma, \\ &2\alpha > a_2. \end{aligned} \tag{5}$$

Dynamics of the binary model can be easily predicted by comparison of the time intervals $(\Delta\tau_i, i=1,2)$ required for each cell to reach the nearest limit point y_i^{LP}:

$$\Delta\tau_i^+ = -\log\frac{y_i^{LP}}{y_i}, \quad \Delta\tau_i^- = -\log\frac{y_i^{LP} - 2\alpha}{y_i - 2\alpha}.$$

The signs "+" and "−" correspond to the upper and lower branches, respectively. The conducted analysis revealed that within domain (5), upon varying a parameter the system exhibits a sequence of bifurcations leading to formation of regular $1:n$ solutions (i.e., one oscillation of the excitable cell 1 is coupled with n oscillations of the oscillatory cell 2), as well as to chaotic behavior.

The complex oscillations domain (OD) in the (γ,α) plane shows a sequence of bands of regularly locked 1:n oscillations (Fig. 2, solutions up to 1:7 are traced) that tend to asymptotic values with increasing γ (with increasing γ the slope of the intermediate branch of null-curve $F_2(x,y)$ as well as its period of oscillation gradually decrease, so that the oscillation ratio n gradually increases). Subdomains of regular 1:n solutions are separated by gaps in which complex periodic or chaotic oscillations are exhibited.

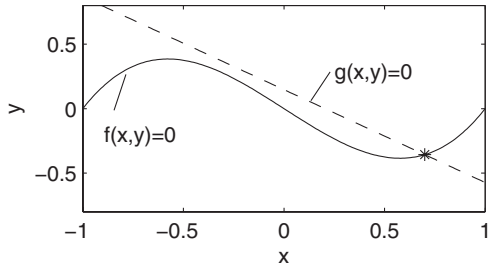

FIG. 3. FHN model [Eqs. (6)–(8)]. The phase plane shows the null clines $f(x,y)=0$ (solid) and $g(x,y)=0$ (dashed). The star marks the selected fixed point.

The OD can be largely predicted from condition (5): For the chosen set of parameters $(a_1=-1, a_2=20, D=1)$, according to conditions (5), the OD is bounded by

$$\alpha > 10, \quad 0.5 < \gamma < 9.5.$$

A similar structure of the OD has been also detected for a pair of identical excitable FHN cells coupled repulsively [10]. This is in principal difference with the behavior of a single excitable cell periodically stimulated by an external fixed force [2], which does not exhibit a chaotic response.

In the case of finite ε we expect to find certain changes of the OD structure (say, an extension of the gaps with aperiodic behavior), as it was detected for a single stimulated EC [2]. The detailed analysis of this problem is beyond the scope of the present paper.

III. DISTRIBUTED FHN SYSTEM

We employ a simple model with a fast distributed activator, and a local (nondiffusing) slow inhibitor,

$$\dot{x} - \Delta x = -x^3 + x + y = f(x,y), \tag{6}$$

$$\dot{y} = \varepsilon(-\alpha x - y + \beta) = g(x,y) \tag{7}$$

subject to the following boundary conditions

$$\xi = 0: \partial x/\partial \xi = 0, \quad \xi = L: \partial x/\partial \xi = \gamma(x - x_w), \tag{8}$$

where ξ denotes the spatial or radial coordinate in a planar case or in a disk, respectively. The diffusion coefficient (D) is set to unity in Eq. (6) after rescaling the length with respect to $\sqrt{D}$, while the dimensionless system length is L.

We set the fixed point [FP, (x_s, y_s)] of the dynamic system, governed by ODE, at the upper branch of the null-curve $f(x,y)$ $(x_s^+=0.7, y_s=x_s^3-x_s$, Fig. 3) and vary parameters α and β simultaneously $(\beta=\alpha x_s+y_s)$ in order to keep the FP. For such a set of parameters the dynamic model possesses three FP's ($x_s^\pm$ and x_s^0) when $\alpha \le \alpha_1 \simeq 0.6325$ and a single FP when $\alpha > \alpha_1$ (Fig. 3). The x_s^+ state is excitable, x_s^0 is a saddle point and x_s^- admits a Hopf bifurcation at $\alpha_H = 1-(x_s^+)^2-(x_H)^2 - x_s^+ x_H \simeq 0.5933$ with $x_H = -\sqrt{(1-\varepsilon)/3}$.

Numerical simulations of a one-dimensional (1D) Cartesian system of sufficiently large L revealed a $U-$ shaped oscillatory domain (OD) in the (α,γ) and (α,x_w) planes [Figs. 4(a)–4(c)] which lies within the domain of excitability $(\hat{\alpha} < \alpha < \tilde{\alpha})$ and above the corresponding threshold values $\gamma^*(\alpha,x_w)$ and $x_w^*(\alpha,\gamma)$. (Most simulations were conducted with $L=160$, a value for which the obtained results appear to be insensitive to L).

The structure of the OD is as follows.

(i) Patterns with a source point (SP) are sustained within a very narrow subdomain adjacent to the low-α boundary of the OD which is practically invisible in Fig. 4. At the low-α boundary of the OD with the threshold value $\hat{\alpha} \simeq \alpha_H$ the stationary quasi-homogeneous solution (with $x(\xi) \in [x_s^-, x_w]$) bifurcates to moving patterns with a narrow front separating domains of $x=x_s^+$ and $x=x_s^-$, that is bouncing from both boundaries [Fig. 5(a)]. With $\alpha > \hat{\alpha}$ two ignition fronts are born at the SP and propagate in opposite directions [Fig. 5(b)]. The left propagating front leaves the system via the no-flux ("homogeneous") boundary, while the right propagating front is reflected from the "inhomogeneous" $(\xi=L)$ boundary. With increasing α the SP moves from the left boundary (with $\alpha=\hat{\alpha}$) towards the "inhomogeneous" boundary $\xi=L$.

(ii) Subdomain of moving pulse solutions (MP) of $m:n$ structure, where m and n denote the number of temporal

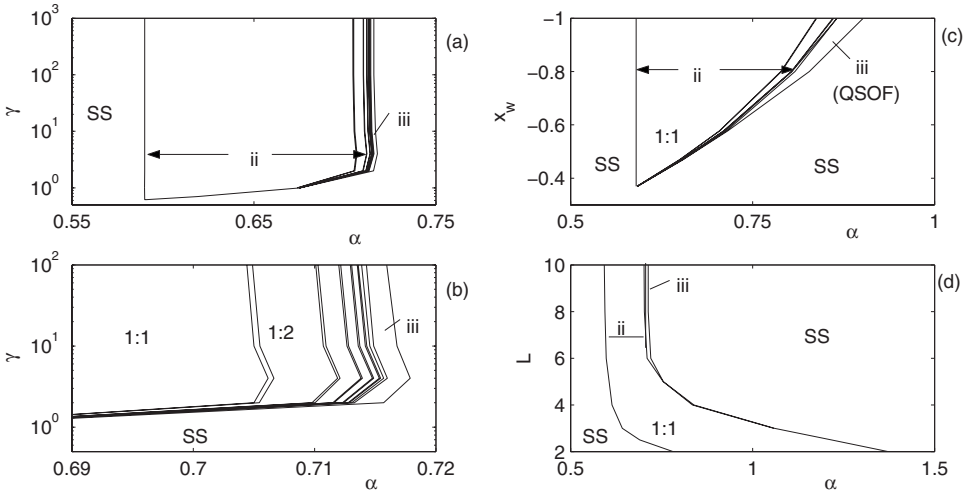

FIG. 4. FHN model [Eqs. (6)–(8)]. The structure of the oscillatory domain in the (γ,α) plane $[x_w=-1/\sqrt{3}$ (a)], (x_w,α) plane $[\gamma=100$ (c)], and (L,α) plane $[x_w=-1/\sqrt{3}$ and $\gamma=100$ (d)] showing subdomains (ii) of moving pulses and subdomain (iii) of quasistationary oscillating front (QSOF) solutions. Plate (b) is an enlargement of plate (a). Numbers show the type of MP solution. Solutions up to 1:7 are traced. $\varepsilon=0.1$; $x_w=-1\sqrt{3}$ in plates (a), (b), and (d), $\gamma=100$ in (c) and (d); and $L=160$ in (a)–(c).

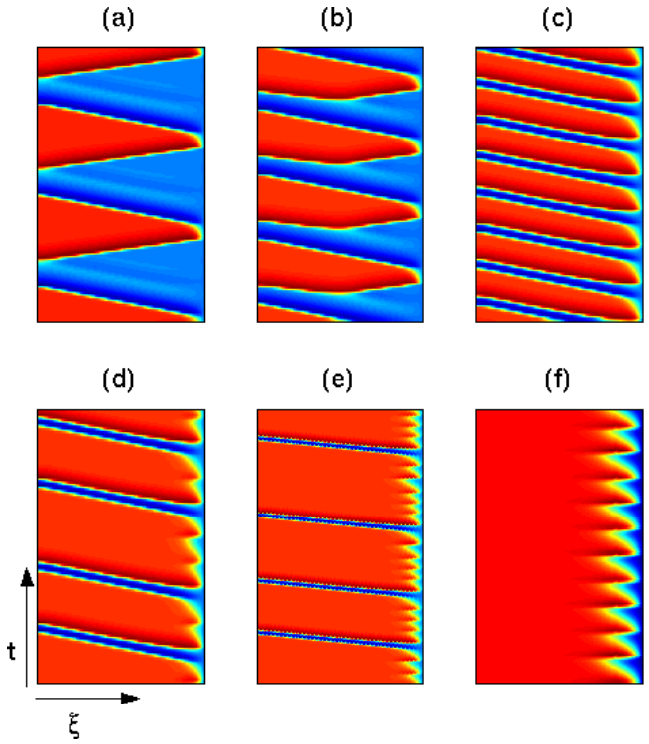

FIG. 5. (Color online) A typical bifurcation sequence of spatiotemporal x pattern of the FHN model [Eqs. (6)–(8)] with varying parameter α in a long system: Pattern with a bouncing front [$\alpha=0.59$ (a)], moving pulses (MP) with a source point [0.592 (b)]; regular MP of a simple structure of 1:1 type [0.70 (c)], and with alternated locking of (1:2)(1:3) type [0.7025 (d)]; aperiodic MP [0.7130 (e)]; a quasistationary pattern with a period-two oscillating front [0.71438 (f)]. In plate (f) the right half of the computational domain is plotted. $\varepsilon=0.1$, $\gamma=100$, $x_w=-1/\sqrt{3}$, and $L=40$.

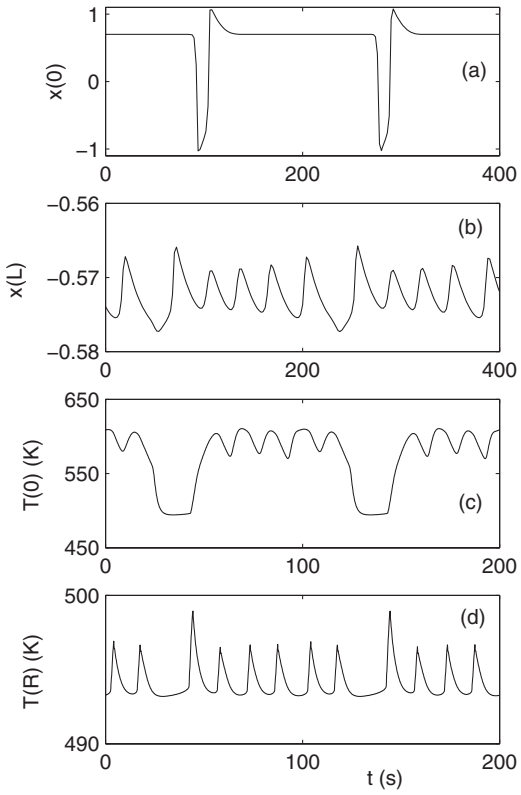

FIG. 6. Typical temporal profiles of complex solutions simulated with FHN model [Eqs. (6)–(8) (a), (b)] and CO oxidation system [Eqs. (9)–(14) (c), (d)]. Plates (a), (b) show x profiles of a 1:5 solution at the no-flux boundary [$x(0)$ (a)] and at the inhomogeneous boundary [$x(L)$ (b)]. $\alpha=0.713$, $L=160$, $x_w=-1/\sqrt{3}$, and $\gamma=100$. Plates (c) and (d) show temperature profiles of a 1:6 solution at the center of the disk [$T(0)$ (c)] and at its boundary [$T(R)$ (d)]. $\gamma=37.5$, $P^0_{CO}=760$ Pa, and $T_g=493$ K; the other parameters as in Ref. [24].

oscillations in the central part of the system and at the boundary where the inhomogeneous BC are applied [Figs. 4 and 5(c)–5(e)], occupies the central and the largest part of the OD.

(iii) A quasistationary pseudohomogeneous solution, with $x(\xi)=x_s^+$ for most part of the region with a sharp oscillating front near the boundary $\xi=L$ [QSOF, Figs. 4 and 5(f)], is sustained within a subdomain adjacent to the high-α boundary of the OD. Just above that subdomain the system exhibits a stationary solution.

Let us focus on the system behavior within subdomain (ii). The state variables exhibit small-amplitude spatiotemporal oscillations in the vicinity of the right boundary $\xi=L$. Some of these oscillations will induce a traveling pulse that moves through most part of the computational domain forming a spatiotemporal pattern of $m:n$ type. A typical 1:5 moving pulse solution is illustrated by Figs. 6(a) and 6(b). At the central part of the computational domain including the left ("homogeneous") boundary the state variables are at the fixed point (x_s^+, y_s^+) for most part of the oscillation cycle. In the vicinity of the "inhomogeneous" boundary the state variables exhibit small amplitude oscillations with x around x_w. The average frequency of these fast oscillations is about the order of the Hopf frequency $\omega_H=\sqrt{\varepsilon(\alpha-\varepsilon)}$ of a single oscillator which does not depend on the fixed point parameters. With increasing γ the amplitude of such oscillations gradually decreases, while the type oscillations is practically preserved at high γ [Fig. 4(a)].

Regular transitions between $(1:n)$ and $(1:n+1)$ patterns occur only through solutions of $(1:n)^k(1:n+1)$ type (i.e., one oscillation of $(1:n+1)$ type is coupled with k oscillations of $(1:n)$ type) and k gradually decreases towards $(1:n+1)$ subdomain. Such a structure was obtained, for example, at the $(1:2)\rightarrow(1:3)$ transition. Alternatively, within the gap of irregular behavior, patterns with arbitrary oscillation ratios can be found. For example within the gap $(1:5)\rightarrow(1:6)$ a rich variety of solutions including $(1:5)(1:4)(1:7)$, $(1:5)^2(1:7)$, $(1:6)(1:8)(1:7)(1:9)$ and even chaotic structures have been detected.

The same three domains (i)–(iii) are evident in the (x_w, α) plane [Fig. 4(c)]. Note, that the threshold value x_w that defines the lower boundary of the OD belongs either to the intermediate or to the stable branch of the null-curve $f(x,y)=0$, opposite to the branch with the fixed point x_s. With increasing $|x_s-x_w|$ deviation the right α boundary of the OD is gradually shifted toward larger α and tends to a certain asymptotic value.

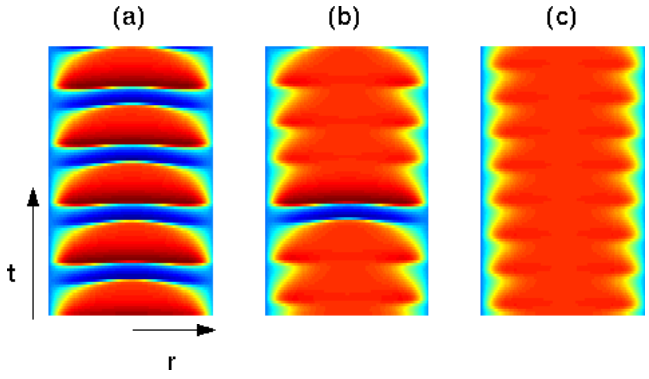

FIG. 7. (Color online) Typical bifurcation sequence of spatiotemporal x pattern of the FHN model [Eqs. (6)–(8)] on a disk with varying parameter α: Standing spots [α=0.78 (a)]; regular oscillations of 1:4 type [0.805 (b)]; continuously breathing oscillations [0.81 (c)]. R=10; the other parameters as in Figs. 6(a) and 6(b).

The velocity of the moving pulses (C_f) is defined mainly by the lumped (ODE) system parameters (see, for example Ref. [26]) and practically is not affected by the applied BC. So the spatial period of oscillations can be estimated by the velocity C_f and the global period of the temporal oscillations.

Now we consider the pattern transformation within subdomain (iii). Numerical simulations revealed that with varying a parameter towards the nearest boundary of subdomain (ii), the QSOF solution exhibits a sequence of period-doubling bifurcations of small-amplitude oscillations in the vicinity of the right boundary ξ=L. This process is accompanied by formation of a quasistationary (for most part of the computational domain) pattern with chaotically oscillating front in the vicinity of ξ=L.

We conclude by briefly considering the effect of the system length L. The existence of a critical L that supports oscillations was derived analytically for a case of an oscillatory media with Dirichlet BC (i.e., x_w=x_s, [24]). This is not possible in the present case of an excitable media with inhomogeneous BC and the threshold L was determined numerically [Fig. 4(d)]. With increasing L the oscillatory domain is shifted towards the smaller α reaching asymptotic values at large L. For sufficiently small L the pulse solution cannot be developed and the sustained patterns have the form of a standing oscillating spot adjacent to the left (no-flux) boundary.

Numerical 2D simulations on a disk revealed only axisymmetric patterns. For sufficiently large radii (R) these patterns admit, upon varying a parameter, the same bifurcation sequence which was detected for the 1D case and the boundaries of the subdomains practically coincide with those of the 1D system. With decreasing R, as in the planar case, the subdomains of complex patterns are shifted toward largest α (Fig. 7). Note that in the axisymmetric case, due to the essential effect of the no-flux boundary conditions (here the symmetry axis), the inward front propagation can be not only "arrested" (as it takes place in a planar case), but also reversed forming outward ignited front propagation. The patterns within subdomain (iii), especially with sufficiently small R, take a form of breathing patterns [Fig. 7(c)].

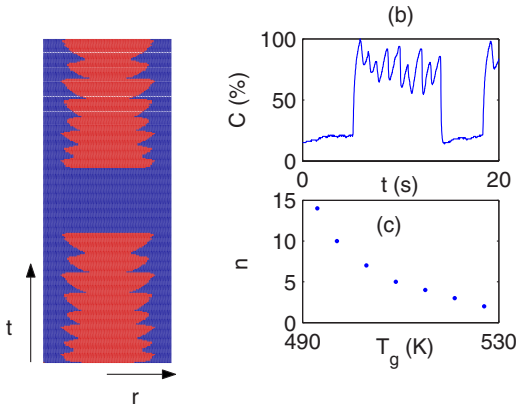

FIG. 8. (Color online) Catalytic CO oxidation experimental results [24] showing the surface temperature pattern [the square root of the active fraction of the disk surface (a)], the effluent product (CO_2) temporal concentration profile (b), and a bifurcation diagram with varying reactor temperature (T_g) showing the number of high-frequency breathing oscillations (n) during the active phase of the cycle (c).

IV. CO-OXIDATION MODEL

In this section we demonstrate that the mechanism producing complex pattern due to inhomogeneous boundary conditions can be extended from the learning FHN model to a more realistic reaction-diffusion model. Catalytic CO oxidation over supported Pd catalyst is a reaction of significant commercial interest (e.g., Ref. [27]). The dynamics of this reaction at atmospheric pressure was intensively studied, both experimentally and numerically, during the past two decades (see, for example, review [28]). This study is motivated by our recently published experimental study of CO oxidation on a disk-shaped catalytic cloth with feed flowing normal and through the cloth [25] showing complex mixed-mode oscillations. The plate holding the catalyst was not catalytic and its temperature was close to the ambient one. Typical IR thermograms exhibit breathing motion, a hot spot which expands and contracts continuously [small-amplitude fast (1 min) oscillations] superimposed on the active phase of the long duration (10–60 min) cycle [Fig. 8(a)]. These oscillations completely map the effluent CO_2 temporal profiles shown in Fig. 8(b). The number of the smaller peaks varied with operating conditions (the reactor temperature) showing a period-adding sequence [Fig. 8(c)]. We analyze here the complex patterns produced by a mathematical model that was previously published by us [29]. We describe first the model and the lumped-system bifurcation diagram followed by the distributed system analysis.

A. Mathematical model and lumped system

The model incorporates three elements: a surface oscillator [Eqs. (9)–(11)], a thermal solid-phase balance assuming that the reactor fluid temperature is fixed and the catalysis is thin [Eq. (12)], and a gas-phase reactor balance. Due to the lack of intercrystallites communication in supported catalysts the surface species are assumed to be not diffusing, so thermal conduction and gas-phase fluxes are the only means of

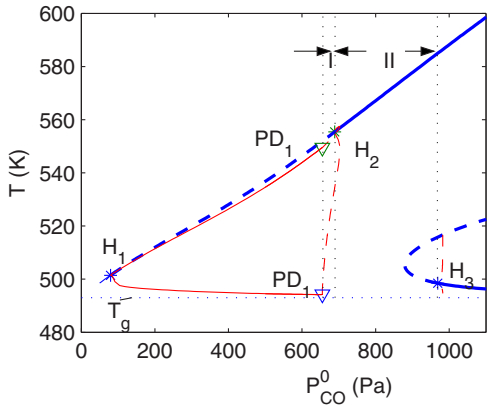

FIG. 9. (Color online) Lumped CO oxidation system [Eqs. (9)–(14) with L_T=0]. Typical bifurcation diagram as a function of the feed CO concentration (P^0_{CO}) showing homogeneous (thick lines) and oscillatory (thin lines) branches. Solid and dashed lines correspond to stable and unstable solutions, respectively. H_i mark the Hopf bifurcation points; PD_1 is period-doubling. Complex oscillations appear in domain I in the lumped system and in domains I and II in the distributed system with imposed homogeneous and inhomogeneous BC, respectively. T_g=493 K; the other parameters as in Ref. [29].

interaction. To write correct balances we should account for gas-phase diffusion (or dispersion) in directions parallel and perpendicular to the disk. In order to simplify the analysis we employ a quite realistic mixed model to describe the CO gas-phase balance [Eq. (14)]. The resulting balance equations are of the form

$$\frac{dx}{dt} = k_1 P_{CO}(1-x-y) - k_{-1}x - k_3 xy - k_5 xz, \tag{9}$$

$$\frac{dy}{dt} = k_2 P_{O_2} e^{-\alpha z}(1-x-y)^2 - k_3 xy - k_4 y(1-z), \tag{10}$$

$$\frac{dz}{dt} = k_4 y(1-z) - k_5 xz, \tag{11}$$

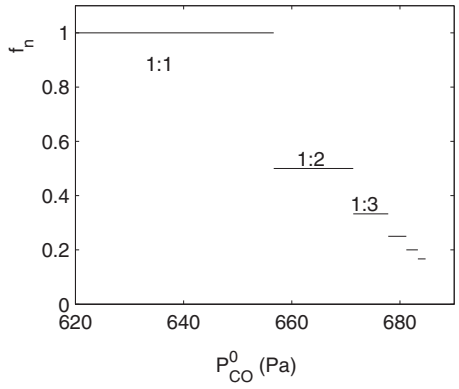

FIG. 10. The structure of the lumped CO oxidation system complex oscillation domain (I in Fig. 9) showing the firing numbers f_n. The parameters as in Fig. 9.

$$\tau_T \frac{\partial T}{\partial t} - L_T^2 \nabla^2 T = (T_g - T) + aR_{CO}, \quad R_{CO} = k_3 xy, \tag{12}$$

$$r=0:\ T_r' = 0, \quad r=R:\ T_r' = \gamma(T_g - T), \tag{13}$$

$$\tau_P \frac{dP_{CO}}{dt} = (P^0_{CO} - P_{CO}) - B^*\langle R'_{CO}\rangle, \quad R'_{CO} = k_1 P_{CO}(1-x-y) - k_{-1}x. \tag{14}$$

Here x and y are the concentration of adsorbed carbon monoxide and adsorbed oxygen respectively; z is the concentration of oxygen in a subsurface layer; T and P_{CO} are the solid temperature (K) and reactant gas phase concentration (Pa), respectively, $\langle\bullet\rangle$ denotes average over the catalyst. The boundary conditions [Eq. (13)] implies heat loss to the circular frame holding the catalysis. The kinetic parameters are those suggested in Ref. [30] with fast activators (x and y) and a slow inhibitor (z). The geometrical, transport and kinetic parameters of the catalyst system were estimated according to experimental data: R=1.8 cm, $L_T=\lambda_s d/h \simeq 0.14$ cm, $\tau_T=\rho_s C_{ps}/h \simeq 2$ s, $B^*=bSRT_{ref}/q=4.62$ s Pa, $a=b(-\Delta H)/h=0.75$ K s, $\tau_P=V/q=0.9$ s (see Ref. [29] for details).

Before studying the disk (distributed) system let us analyze the relevant lumped model ignoring the boundary effects [i.e., without conduction in Eq. (12)]. As was shown in Refs. [32,33] the oscillatory domains of the distributed CO oxidation models, that do not account for the interaction between the local and space average variables (at least in the case of no flux BC), practically coincide with those of the relevant lumped systems. A typical bifurcation diagram of the lumped model (9)–(14) showing the effect of feed CO concentration (P^0_{CO}) presents (Fig. 9, simulated by means of the software package AUTO [34]) a steady isolated (high-temperature) and fold-shaped (low- and middle-temperature) branches. The stable high-temperature branch undergoes a supercritical Hopf bifurcation at point H_1 and subcritical at point H_2, while the low-temperature branch undergoes a subcritical Hopf bifurcation at point H_3. The stable oscillatory branch emanating from H_1 exhibits a period-doubling bifurcation at point PD_1 where it merges with the unstable oscillatory branch emanating from H_2. Within the domain approximately bounded by H_2 and PD_1 (noted by I in Fig. 9) the lumped system exhibits bursting solutions of 1:n type with a global cycle composed of n small-amplitude fast oscillations around the high-temperature steady state coupled with a large-amplitude slow oscillation loop close to the unstable period-one orbit. With varying a parameter these oscillations admit a period-adding bifurcation sequence with a clearly distinguished stair-case structure (Fig. 10). These temporal patterns were previously investigated by us [29,31] and attributed to a canard bifurcation of the reduced four-variable subsystem of the original model which was derived by converting one of the state variable (T) to be a prescribed parameter.

B. Distributed system

We portray the behavior in the (P^0_{CO}, γ) plane. Numerical simulations of the partial differential equation (PDE) system

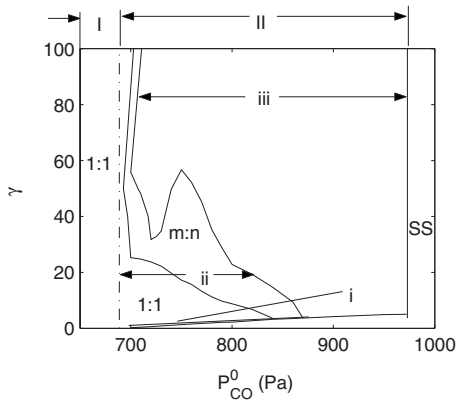

FIG. 11. Distributed CO oxidation system [Eqs. (9)–(14)]. The structure of the oscillatory domain in the (γ, P^0_{CO}) plane showing subdomains of quasihomogeneous oscillations (i), complex mixed-mode oscillations (ii), and breathing patterns (iii). Dashed-dotted line separates domains I and II (Fig. 9). $R=1.8$ cm; the parameters as in Fig. 9.

with the no-flux boundary conditions ($\gamma=0$) yield spatially homogeneous patterns identical to the lumped model solutions, i.e., the system exhibits simple period-one oscillations when $P_{H1}<P^0_{CO}<P_{PD1}$, bursting oscillations within domain I with $P_{PD1}<P^0_{CO}<P_{H2}$ and stationary quasi-homogeneous solutions with $P^0_{CO}>P_{H2}$. Thus, the oscillatory domain of the distributed system (9)–(14) practically coincides with this of the relevant lumped model.

In the case of inhomogeneous BC ($\gamma\neq 0$) a large domain of complex system behavior (noted by II in Fig. 11) emerges within a domain of stable (excitable) states of the corresponding lumped system. As in the case of the FHN model this domain is U- shaped showing clear P^0_{CO} asymptotes when $\gamma\to\infty$ (i.e., fixed-temperature BC).

Within domain II we find three subdomains of qualitatively different behavior: Quasihomogeneous oscillations [QHO, Fig. 12(b), noted by (i) in Fig. 11], complex mixed-mode patterns [Figs. 12(c)–12(e), (ii) in Fig. 11] and breathing patterns [Fig. 12(f), (iii) in Fig. 11]. Note that the two last types were detected also for the FHN model.

The complex spatiotemporal m:n type patterns [Figs. 12(c)–12(e)] exist at moderate γ and admit period-adding bifurcations with varying a parameter. Due to relatively small disk radii (corresponding to experimental conditions) we did not observe fully developed pulse propagation as was obtained using the FHN model. Instead, the system exhibits a sequence of high frequency, breathing oscillations with a hot spot in the central part of the disk separated by intervals of completely extinguished state. Typical 1:6 complex solution is illustrated by Figs. 6(c) and 6(d) showing the temporal profiles of the surface temperature at the disk center (c) and at its boundary (d). Due to the small disk radii small amplitude fast oscillations generated at the boundary do not decay up to the disk center leading to formation of the mixed-mode oscillations on the whole surface.

The number (n) of small amplitude breathing oscillations increases with γ and, as in the case of the learning models, the subdomains of regular $1:n$ oscillations are separated by

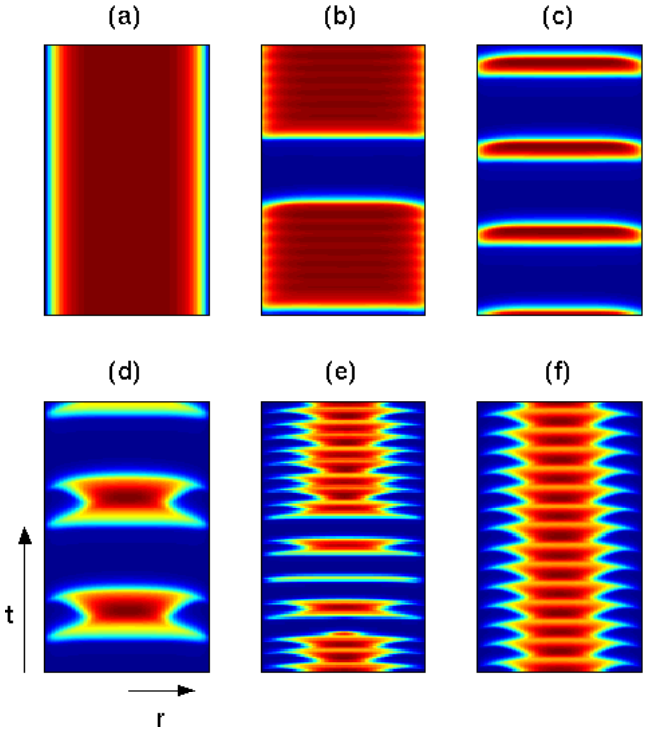

FIG. 12. (Color online) CO oxidation system [Eqs. (9)–(14)]. Typical bifurcation sequence of the spatiotemporal temperature patterns in the distributed system upon increasing γ showing stationary pattern [(a) $\gamma=1.3$], a quasihomogeneous firing pattern of $1:n$ type [(b) $\gamma=1.62$], a period-one pattern [(c) $\gamma=2.5$], a regular 1:3 pattern [(d) $\gamma=10$], an aperiodic oscillations [(e) $\gamma=45$], and a continuous breathing pattern [(f) $\gamma=100$]. $P^0_{CO}=760$ Pa. The other parameters as in Fig. 11.

gaps of more complex and even chaotic behavior. The detection of all internal subdomain boundaries is very time-consuming and is skipped in the present study, especially in view of their high sensitivity to the system parameters, which makes the OD structure nonuniversal.

Continuous breathing patterns [Fig. 12(f)] are detected at high-γ and large P^0_{CO}. These simple period-one oscillations bifurcate with decreasing γ [near the boundary with subdomain (ii)] forming a sequence of aperiodic breathing patterns.

For the set of parameters employed in Fig. 9 domain II is adjacent to domain I of the LM and is approximately bounded by H_2 and H_3 bifurcations. The subdomain of quasihomogeneous oscillations existing at low γ [QHO, Fig. 11, subdomain (i)] emerges due to the properties of the LM. With increasing γ they gradually bifurcate to a simple 1:1 structure.

V. DISCUSSION

We demonstrated that external forcing via boundary effects in a reaction-diffusion excitable system can generate temporally-complex spatiotemporal patterns that are characterized by a period-adding scenario when a parameter is varied. We mapped such a behavior for two continuously dis-

tributed systems with either a cubic autocatalytic kinetics model (FHN) or with a realistic CO oxidation model, when both are subject to a BC of the third type. A similar behavior was mapped for a simple two cell binary model with a piecewise linear kinetics (2CPWK) and we want to explain this similarity.

While the 2CPWK model captures the main features of the excitable FHN model subject to inhomogeneous BC, and both models exhibit domains of frequency-locked solutions separated by gaps of aperiodic (chaotic) behavior, the translation of the former to the later required some explanation, as we do below.

The boundaries of the oscillatory domain of the 2CPWK model [Eqs. (1)–(4)] are defined [Eq. (5)] by the requirement that upon interaction between the cells, the phase plane of cell 1 is shifted from an excitable to an oscillatory state, while the cell 2 oscillatory phase plane is preserved. The model is written in a way that within this domain the "excitability" parameter α and the "boundary" coefficient γ do not affect the *existence* of the limiting points having a constant x_i^{LP} (± 1) and varying y_i^{LP}. Contrary, these parameters affect the period of oscillation: With increasing γ the slope of the intermediate branch of null-curve $F_2(x,y)$ (Fig. 1), as well as its oscillation period and the amplitude $y_2^{LP+}-y_2^{LP-}$ gradually decreases. As the oscillation period tends to zero with $\gamma \to (a_2-a_1-2\mathrm{D})$, we observed condensation of $1:n$ subdomains towards this boundary (Fig. 2).

In the two extended models the effects of the "boundary" coefficient γ and the "excitability" parameter (α in the FHN model and P_{CO}^0 in the CO oxidation model) on the system behavior are qualitatively different since their change affects the form of the null-curves. To illustrate this distinction consider a finite-difference approximation of the 1D FHN system with cubic kinetics (6)–(8):

$$\dot{x}_i - \frac{1}{\Delta}\left(\frac{x_{i+1}-x_i}{\Delta} - \frac{x_i - x_{i-1}}{\Delta}\right) = f(x_i,y_i) + O(\Delta), \quad (15)$$

$$\dot{y}_i = \varepsilon(-\alpha x_i - y_i + \beta) = g(x_i,y_i), \quad i = 1,\ldots,N, \quad (16)$$

$$\frac{x_2 - x_1}{\Delta} = \gamma(x_2 - x_1) + O(\Delta), \quad \frac{x_N - x_{N-1}}{\Delta} = O(\Delta), \quad (17)$$

where N is the number of grid points and $\Delta = L/(N-1)$ is a constant space step. As a first step we employ a three-point mesh ($N=3$) so that point $i=2$ is the only internal point governed by Eqs. (15) and (16). With incorporation of BC (17) into Eq. (15) we obtain

$$\dot{x}_2 = -x_2^3 + x_2\left(1 - \frac{\gamma}{\Delta}\right) + y_2 + \frac{\gamma}{\Delta}x_w = F\left(x_2, y_2, \frac{\gamma}{\Delta}, x_w\right). \quad (18)$$

The limit points of null-curve $F(x_2, y_2, \gamma/\Delta, x_w)=0$ are

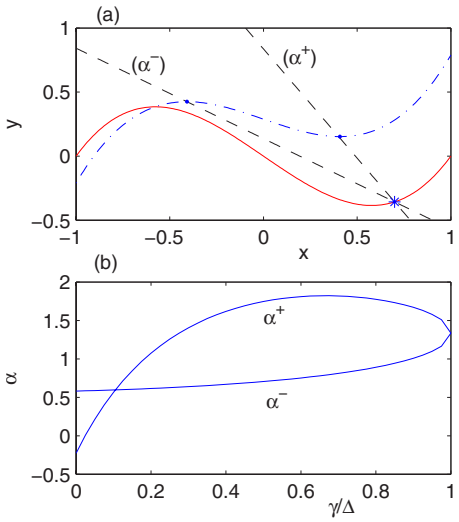

FIG. 13. (Color online) The phase plane transformation of the FHN model due to applied BC. Plate (a) shows the unperturbed null curve $f(x,y)=0$ [Eq. (6), solid lines], shifted null curve $F(x,y,\gamma/\Delta,x_w)=0$ [Eq. (18), dashed-dotted lines], and the $g(x,y)=0$ null curves corresponding to limiting α values [Eq. (20), dashed lines]. The star marks the selected fixed point. Plate (b) shows the OD in the $(\gamma/\Delta,\alpha)$ plane for a case of small γ [Eqs. (18)].

$$x_2^{\pm} = \pm\sqrt{\frac{1-\gamma/\Delta}{3}}, \quad y_2^{\pm} = (x_2^{\pm})^3 - x_2^{\pm}\left(1 - \frac{\gamma}{\Delta}\right) - \frac{\gamma}{\Delta}x_w. \quad (19)$$

Now the necessary condition for cell 2 to be oscillatory can be easily formulated [Fig. 13(a)]:

$$\alpha^- < \alpha < \alpha^+, \quad \alpha^{\pm} = \frac{y_2^{\pm} - y_s}{x_s - x_2^{\pm}}, \quad 0 < \gamma/\Delta < 1, \quad (20)$$

where (x_s, y_s) is the steady state of the isolated (excitable) system. A typical lentil-like domain of the oscillatory solution in the $(\gamma/\Delta,\alpha)$ plane is shown in Fig. 13(b) (within the left subdomain with $\alpha^+ < \alpha < \alpha^-$ Eq. (18) admits three steady state solutions).

Next, we can extend the grid up to $N=4$ with two internal points (2 and 3). After incorporation of BC (17) into appropriate Eq. (15) we obtain a two-cell system similar to model Eqs. (1)–(4) with the exception of the nonlinear source terms. Comparison of this two-cell model with that of 2CPWK shows that while γ plays a similar role, its effect on the limit points is quite different.

In the limiting $\gamma \to \infty$ case "inhomogeneous" BC (17) should be replaced by $x_1 = x_w$, while coefficient γ in Eqs. (15)–(20) should be replaced by $1/\Delta$. Hence we can find both lower and upper α boundaries of the OD with respect to parameter $1/\Delta^2$ [instead of γ/Δ, Fig. 13(b)]. As these values do not depend on γ, we can suggest that the boundaries of the OD tend to certain asymptotic values with $\gamma \to \infty$. The conducted analysis explains the U-shaped form of the OD (Figs. 4 and 11) in the (parameter, γ) plane bounded by two asymptotes that persist as $\gamma \to \infty$, and by a low-γ boundary

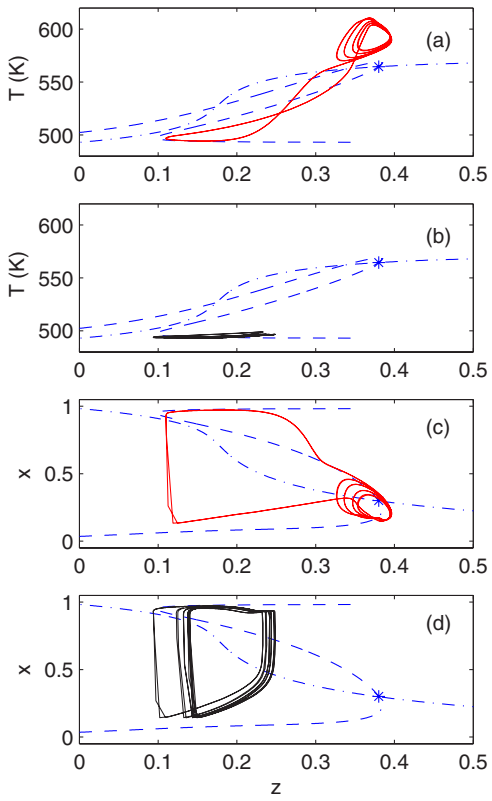

FIG. 14. (Color online) CO oxidation model [Eqs. (9)–(14)]. Typical lumped system phase plane projections of "fast" [Eqs. (9), (10), (12), and (14), dashed-dotted lines] and "slow" [Eqs. (9), (11), (12), and (14), dashed lines] null curves on $[z,T$ (a), (b)] and $[z,x$ (c), (d)] planes. Solid lines show typical simulated (1:5) PDE solution at the disk center [(a), (c)] and at its boundary [(b), (d)]. The parameters are as in Figs. 6(c) and 6(d). The star marks the fixed point [additional intersections are obtained as projections of twisted curves on a plane and do not correspond to any fixed point].

since for $\gamma=0$ (no-flux BC) the system is excitable and exhibits a stationary solution.

Next we show the commonality of the CO oxidation and the FHN models. The x,y surface species in the former exhibit bistability with respect to z species, and their interaction produces relaxation oscillation with wide (three orders of magnitude) separation of time scales. The state variables x,y and z are not diffusing and the communication is mediated by conduction (the enthalpy balance) and mixing (mass balances); an interaction between local and space average variables, such as that described by Eq. (14) can also affect the pattern selection mechanism. Due to large time scale separation we can conduct a simplified qualitative phase plane analysis of the relevant ODE system using its fast [Eqs. (9), (10), (12), and (14)] and slow [Eqs. (9), (11), (12), and (14)] subsets. Typical phase plane projections on (z,T) and (z,x) planes constructed in such a way are shown in Fig. 14 ("fast" and "slow" null curves are shown by solid and dashed lines correspondingly). The steady state solution (denoted by the star in Fig. 14) is stable following the bifurcation map of Fig. 9 and the corresponding phase plane can be described as excitable.

The comprehensive analysis of the full five variable system (9)–(14) with account for global coupling is very complicated, and as a fist step we can consider a modified system assuming that the gas-phase mixing is absent [instead of the spatially average source term in Eq. (14)]. To get some insight into the BC effect we can incorporate an additional term $\frac{\gamma}{\Delta}(T-T_g)$ into the finite-difference approximation of Eq. (12) following the approach described above [Eq. (18)] and to repeat the procedure. The conducted analysis shows that upon increasing γ/Δ the corresponding phase plane can exhibit up to three fixed points and is highly sensitive to the state parameters (particularly to the "excitability" parameter P^0_{CO}). Thus, we can reasonably expect a qualitative realignment of the system behavior and transformation from the stationary solution (with $\gamma=0$) to a certain pattern state with $\gamma>0$. To ascertain that global coupling is not the source of the complex pattern formation we ran additional simulations (assuming no gas-phase mixing) and using the same set of parameters. These simulations revealed a sequence of moving pulse solutions of a $1:n$ structure typical for long systems which admits period adding bifurcations within the $(P^0_{\mathrm{CO}}, \gamma)$ OD of a modified structure with respect this of Fig. 11. Comparison of these results with simulations of the original model allows to conclude that for condition under consideration global coupling leads to a certain equalization of variables at least at the central part of the disk (formation of breathing patterns) and shifting of the oscillatory subdomain boundaries, but do not change the mechanism of the complex pattern formation due to the boundary effects.

Typical phase plane trajectories of the complex pattern solution of original system (9)–(14) are shown in Fig. 14. In the disk center the trajectory is composed of a large amplitude loop for all state variables and several small amplitude loops close to the steady state. Near the disk boundary the phase trajectory exhibits small amplitude loops with respect to the diffusive variable (T) for which the BC are imposed [Fig. 14(b)]. Upon varying a parameter the number of small amplitude loops is varied both in the disk center and at its boundary. Such phase planes are also typical for the classical FHN model simulated in Sec. III. The complex form of the $(P^0_{\mathrm{CO}}, \gamma)$ bifurcation map as opposed to the relatively simple FHN bifurcation diagrams is probably due to the more complex five-variable system behavior (compare Fig. 3 and Fig. 14).

Summarizing the obtained results with continuously distributed models we can conclude that the structure of the oscillatory domain in the (α,γ) or $(P_{\mathrm{CO}}, \gamma)$ planes is U-shaped due to two asymptotes of strong BC $(\gamma\to\infty, x\to x_w, T\to T_w)$ and a lower γ-boundary since for $\gamma=0$ the system exhibits homogeneous solutions. Numerical simulations of the FHN and the CO-oxidation models revealed two types of complex patterns which seem to be generic for distributed excitable systems subject to inhomogeneous boundary conditions.

(1) Temporal m:n structures with the boundary sending moving pulses [subdomain (ii)]; it consists of wide subdomains of regular $1:n$ patterns separated by gaps of more complex and even chaotic behavior.

(2) Continuously breathing regular or aperiodic patterns with an oscillating front [subdomain (iii)].

Finally we would like to point out that the numerically simulated patterns within subdomain (ii) of the CO oxidation model qualitatively match our experimental observations of CO catalytic oxidation on a disk [25] [compare Fig. 8(a) and Fig. 12(e)]. To get a good quantitative agreement a certain parameter adjustment is required, which can be easily justified as most of the kinetic constants (as well as the catalyst properties) are not known exactly.

ACKNOWLEDGMENTS

This work is supported by US-Israel BSF. O.N. is partially supported by the Center for Absorption in Science, Ministry of Immigrant Absorption State of Israel. M.S. is a member of the Minerva Center of Nonlinear Dynamics and Complex Systems.

[1] O. Nekhamkina and M. Sheintuch, Phys. Rev. E **73**, 066224 (2006).
[2] S. Coombes and A. H. Osbaldestin, Phys. Rev. E **62**, 4057 (2000).
[3] D. T. Kaplan, J. R. Clay, T. Manning, L. Glass, M. R. Guevara, and A. Shrier, Phys. Rev. Lett. **76**, 4074 (1996).
[4] J. R. Clay, J. Comput. Neurosci. **15**, 43 (2003).
[5] T. Yanagita, Y. Nishiura, and R. Kobayashi, Phys. Rev. E **71**, 036226 (2005).
[6] A. Carpio, Physica D **207**, 117 (2005).
[7] H. Fujii and I. Tsuda, Lect. Notes Comput. Sci. **3146**, 140 (2004).
[8] K. Tateno, H. Tomonari, H. Hayashi, and S. Ishizuka, Int. J. Bifurcation Chaos Appl. Sci. Eng. **14**, 1559 (2004).
[9] D. Paz'o and E. Montbri'o, Phys. Rev. E **73**, 055202(R) (2006).
[10] T. Yanagita, T. Ichinomiya, and Y. Oyama, Phys. Rev. E **72**, 056218 (2005).
[11] J. Krishnan, I. G. Kevrekidis, M. Or-Guil, M. G. Zimmerman, and B. Markus, Comput. Methods Appl. Mech. Eng. **170**, 253 (1999).
[12] M. Or-Guil, I. G. Kevrekidis, and M. Bar, Physica D **135**, 154 (2000).
[13] G. Bordiougov and H. Engel, Phys. Rev. Lett. **90**, 148302 (2003).
[14] B. Lindner, J. Garcia-Ojalvo, A. Neiman, and L. Scimansky-Geier, Phys. Rep. **392**, 321 (2004).
[15] M. Perc, Phys. Rev. E **72**, 016207 (2005).
[16] S. Bouzat and H. S. Wio, Phys. Lett. A **268**, 323 (2000).
[17] S. E. Folias and P. C. Bressloff, Phys. Rev. Lett. **95**, 208107 (2005).
[18] A. Prat, Y.-X. Lia, and P. Bressloff, Physica D **202**, 177 (2005).
[19] T. R. Chigwada, P. Parmananda, and K. Showalter, Phys. Rev. Lett. **96**, 244101 (2006).
[20] V. M Eguíluz, E. Hernández-García, and O. Piro, Physica A **283**, 48 (2000).
[21] J. I. Ramos, Appl. Math. Comput. **146**, 55 (2003).
[22] R. Wackerbauer and K. Showalter, Phys. Rev. Lett. **91**, 174103 (2003).
[23] S. Bouzat and H. S. Wio, Physica A **317**, 472 (2003).
[24] A. Rabinovitch, M. Gutman, and I. Aviram, Phys. Rev. E **67**, 036212 (2003).
[25] R. Digilov, O. Nekhamkina, and M. Sheintuch, AIChE J. **50**, 163 (2004).
[26] E. Meron, Phys. Rep. **218**, 1 (1992).
[27] M. Sheintuch, J. Schmidt, Y. Lechthman, and G. Yahav, Appl. Catal. **49**, 55 (1989).
[28] D. Luss and M. Sheintuch, Catal. Today **105**, 254 (2005).
[29] O. Nekhamkina, R. Digilov, and M. Sheintuch, J. Chem. Phys. **119**, 2322 (2003).
[30] M. M. Slin'ko, E. S. Kurkina, M. A. Liauw, and N. I. Jaeger, J. Chem. Phys. **111**, 8105 (1999).
[31] O. Nekhamkina, R. Digilov, and M. Sheintuch, *Eighth Experimental Chaos Conference*, AIP Conf. Proc., No. 742 (AIP, New York, 2004), pp. 15–20.
[32] O. Nekhamkina and M. Sheintuch, J. Chem. Phys. **122**, 194701 (2005).
[33] G. A. Viswanathan and D. Luss, AIChE J. **52**, 705 (2006).
[34] E. J. Doedel, Congr. Numer. **30**, 265 (1981).